Remote measurements of magnetospheric Energetic Neutral Emissions by the Interstellar Boundary Explorer: Probing dayside and nightside processes

IBEX Data Release 12

The fortuitous combination of the Interstellar Boundary Explorer (IBEX) mission parameters: highly eccentric equatorial earth orbit, sun-pointing spinner, and highly sensitive energetic neutral atom (ENA) instruments with field-of-view perpendicular to the spin axis, form a perfect platform to observe ENA emissions from the Earth's magnetosphere for long periods of time and from distances up to ~50 earth radii. IBEX views the magnetosphere from the side making continuous ~7° x 360° vertical swaths of the sky (great circle scan) at a resolution of ~14 seconds per full swath, covering an overlapping energy range of ~0.01 to ~1.8 keV (IBEX-Lo) and ~0.3 to ~6 keV (IBEX-Hi). These swaths, which convolve spatial and temporal information, are used to construct composite ENA images of the Earth's magnetosphere for different solar wind and interplanetary magnetic field conditions.

This release provides, for the first time, a validated set of orbits that supported 7 studies over the last few years, a detailed data description, and highlights IBEX magnetospheric science capabilities and some of the challenges associated with this data set. The data comprises 18 orbits from IBEX-Hi 6° histogram ENA count data, which are primarily what have been used in IBEX magnetospheric studies. This data release demonstrates that IBEX provides a unique global viewing perspective of the magnetosphere that complements in situ measurements in understanding magnetospheric plasma regions and processes on micro and macro scales.

The release is separated into four sections, as follows:

1. **IBEX orbital configuration**: provides orbital information about IBEX and describes how it is able to image the Earth's magnetosphere.
2. **Associated publications**: outlines the publications that have validated and used this data set.
3. **Data description**: provides details about the treatment of IBEX magnetospheric data.
4. **Data**: includes data in ASCII format for the 18 orbits provided in this release as well as accompanying browse plots.

1. IBEX orbital configuration

As IBEX's orbit precesses around Earth during the latter's journey around the sun, IBEX views the magnetosphere from the dawn and dusk sides for long periods of time. Figure 1 shows the geometry of IBEX's orbit and magnetospheric viewing times during 2009. Magnetospheric viewing times are good for about ~6 months per year, covering dayside (red bands along the orbit) and nightside (blue bands along the orbit) viewing of the inner and outer magnetosphere regions. Orbital configurations for equinox and solstice times are also shown.

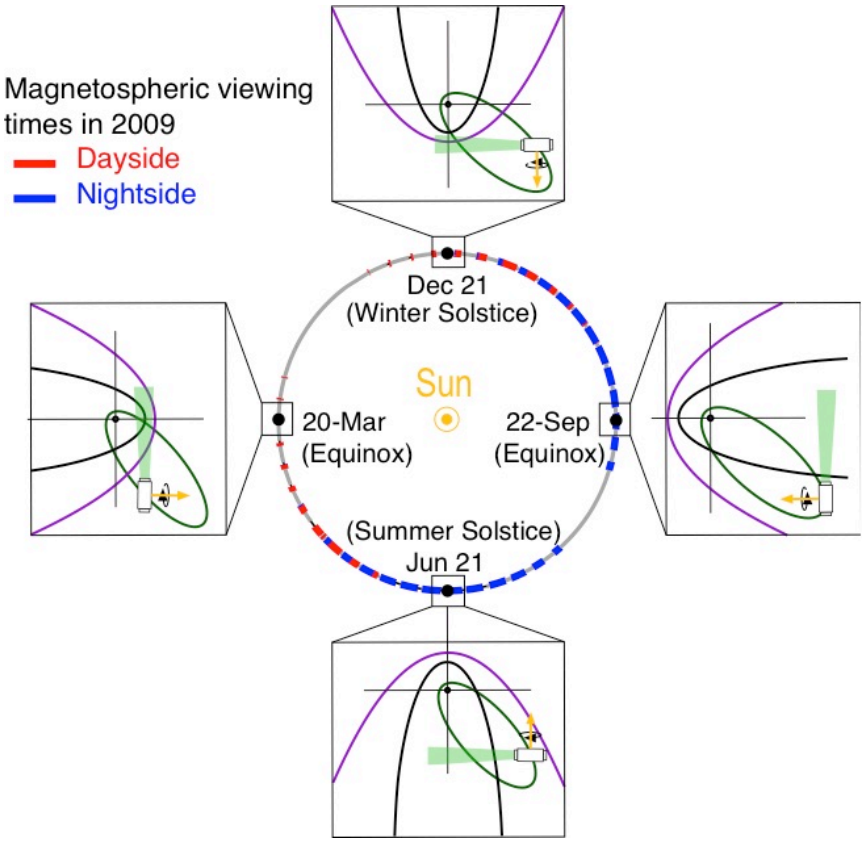

Figure 1

For the first two and a half years of science operations (through Orbit 127), IBEX's orbital period was ~7.5 days and the spin axis was repointed once each orbit (around perigee), leading to bands of sky viewing centered 7.5° apart. In June 2011, over Orbits 128 and 129, IBEX was maneuvered into a previously unknown, long-term stable lunar synchronous orbit with apogee still ~50 R_E (McComas et al. 2011a). Since then, IBEX's orbital period has been ~9.1 days (one-third of the lunar sidereal period of 27.3 days). Orbit numbers from 130 onward are split into two segments, 'a' and 'b.' Furthermore, starting in orbit segment 184a, we modified the IBEX-Hi energy step sequence and eliminated the lowest energy step (ESA1) in exchange for doubling the statistical sampling of ESA3 (center energy ~1.1 keV).

Figure 2 shows Two IBEX orbit configurations illustrating its magnetospheric viewing before (blue) and after (red) the perigee maneuver by which IBEX was placed into a more stable orbit. Highly elliptical orbit configurations provide imaging of distant magnetospheric regions for a significant amount of time. This figure shows enhanced emissions at two different energies from the magnetopause and cusps during the dayside viewing, and from the plasma sheet during the nightside viewing.

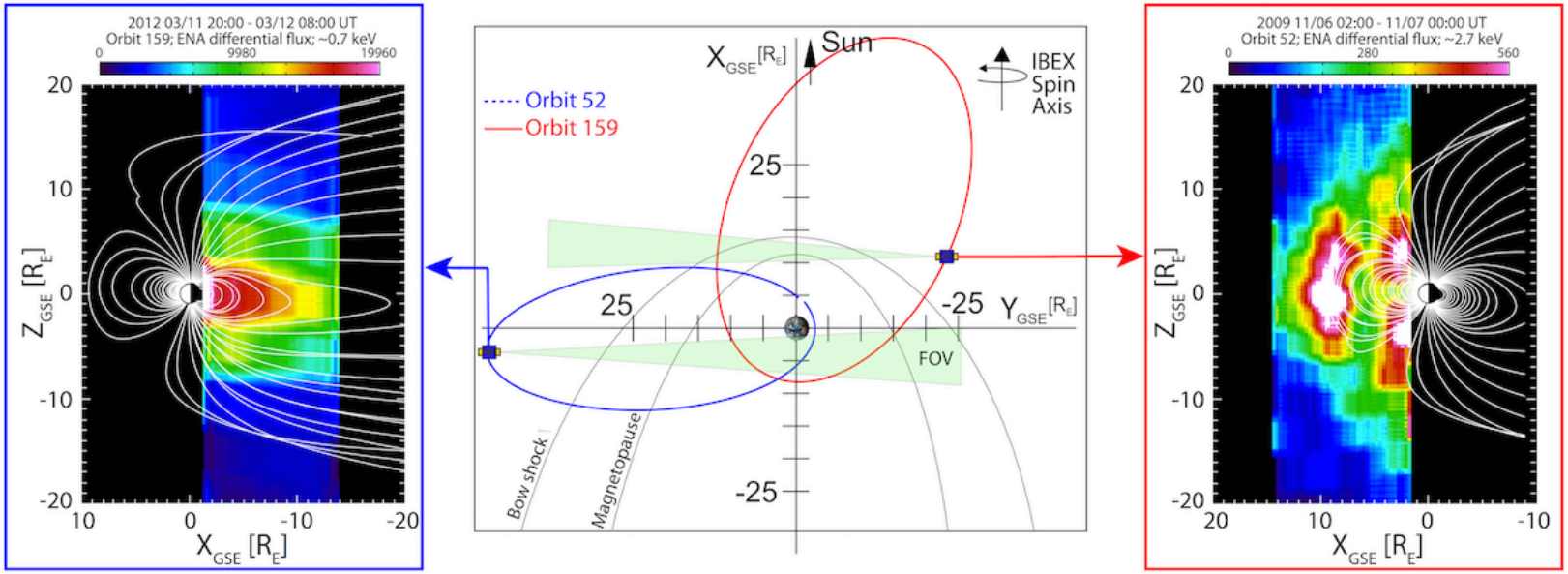

Figure 2

2. Associated publications

Study Title	Reference	Orbits
Energetic neutral atoms from the Earth's subsolar magnetopause	Fuselier et al. (2010), Geophys. Res. Lett., 37, L13101.	21* 23 24 25
First IBEX observations of the terrestrial plasma sheet and a possible disconnection event	McComas et al. (2011), J. Geophys. Res., 116, A02211.	51 52
Neutral atom imaging of the magnetospheric cusps	Petrinec et al. (2011), J. Geophys. Res., 116, A07203.	23 25 27 53 55 56 57 74 77 78
Two Wide-Angle Imaging Neutral-Atom Spectrometers and Interstellar Boundary Explorer energetic neutral atom imaging of the 5 April 2010 substorm	McComas et al. (2012), J. Geophys. Res., 117, A03225.	72
Characterizing the dayside magnetosheath using energetic neutral atoms: IBEX and THEMIS observations	Ogasawara et al. (2013), J. Geophys. Res. Space Physics, 118, 3126–3137.	103
Imaging the development of the cold dense plasma sheet	Fuselier et al. (2015), Geophys. Res. Lett., 42, 7867–7873.	206a
Shape of the terrestrial plasma sheet in the near-Earth magnetospheric tail as imaged by the Interstellar	Dayeh et al. (2015), Geophys. Res. Lett., 42,	29 188b

Boundary Explorer 2115–2122.

*A significant portion of this orbit has some issues with pointing information. Further validation will be performed throughout the orbit for a possible later release.

3. Data Description

- This data release comprises 18 orbits which supported 7 published studies over the last few years. The orbits cover nightside and dayside viewing by IBEX.
- For each orbit, there are 5 ASCII files representing 5 different energies that correspond to IBEX-Hi ENA measurements at ~0.71, ~1.11, ~1.74, ~2.73, and ~4.3 keV.
- The data are arranged in 6-degree bins in the spin phase (for each spin, there are 60 6-degree bins covering the 360 degree view).
- Each data file includes timing, spacecraft and object ephemeris, and spacecraft pointing information along with the ENA skymap time vs Counts in 6-degree bins covering 360 degrees. ENA counts are binned every 96 spins over the whole sky.
- A complete energy sweep over all energy bands is done every 12 spins (sweeping sequence: 1,1-2,2-3,3-4,4-5,5-6,6. This changed to 2,2-3,3,3,3-4,4-5,5-6,6 at the beginning of orbit segment 184a as indicated earlier). For this dataset, each swath is accumulated every 96 spins, so the exposure time per 6° bin per energy is:

  (96 spins/6 energy bins) * (time-per-spin)/60 bins).

- The magnetospheric composite images are created using the ephemeris and pointing information to project the measured ENAs onto the XZ plane.
- For each orbit, we also provide a browse plot that shows the 5 ENA maps at all energies, orbital configuration, and a sample projection of ENAs (at ~1.7 keV) onto the XZ (GSE) plane. Figure 3 below shows a sample browse plot followed by the panels description.

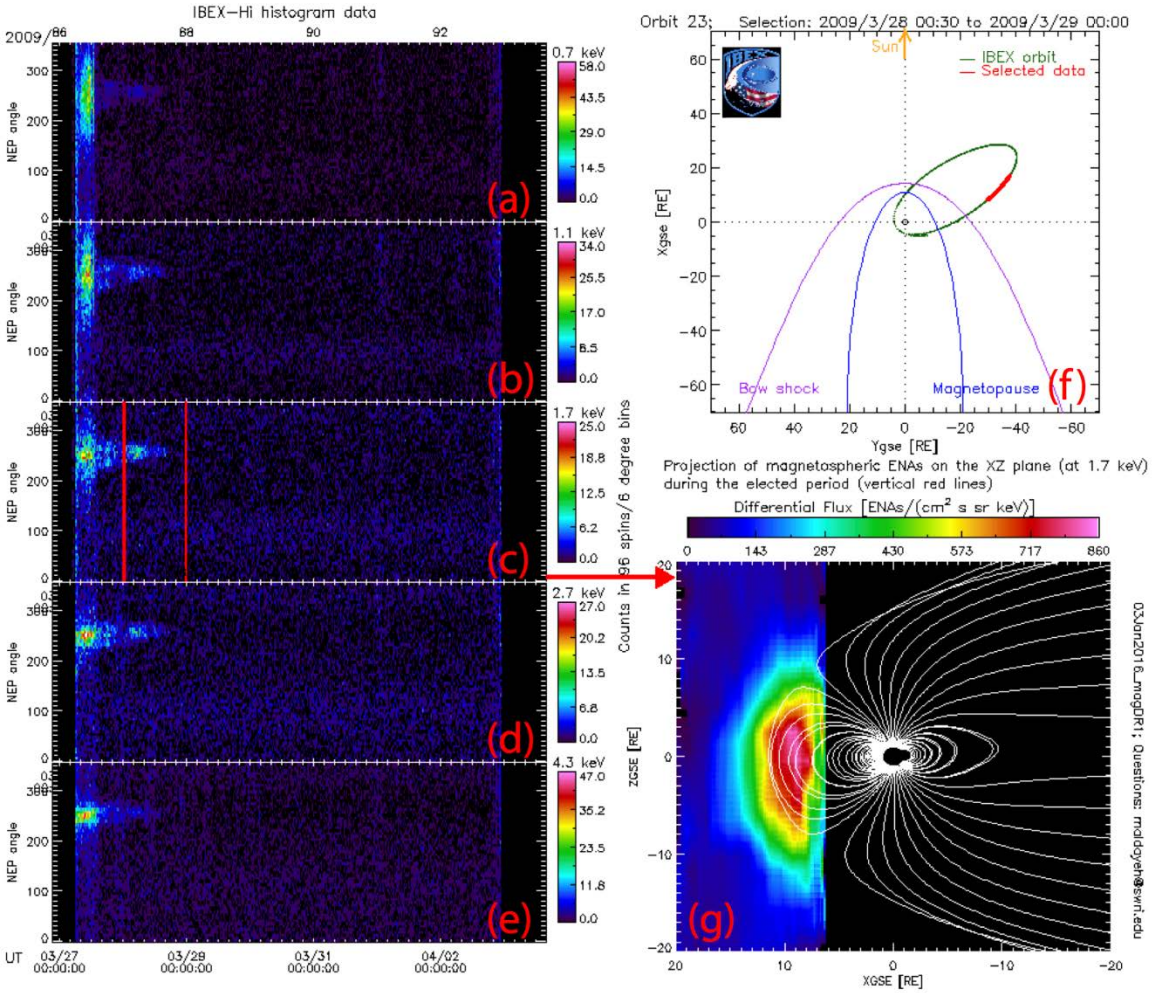

Figure 3: (a)-through (e): ENA skymaps at 5 energies. Enhanced emissions from the magnetosphere are clear and centered at around ~270 degrees. The vertical enhanced ENA swath early in the orbit is due to the deflected solar wind when IBEX is located in the magnetosheath. Note that the heliospheric ribbon is the broad faint ENA glow centered at ~100 degrees. The vertical lines in (c) indicate the time period selected in this orbit. (f) Orbital configuration of IBEX. Red traces correspond to IBEX location during the selected time period. (g) Composite ENA image of magnetospheric emissions acquired during ~24

hours. Tsyganenko field lines are over plotted for reference. Disclaimer: These images convolve temporal and spatial variations. User should be very careful interpreting the results. In some cases, the projection software shows projection artifacts that are not necessarily realistic.

3.1 Converting Counts to Fluxes

- ENA flux J(E) at energy E can be derived from the count rate C using the following formula:

$$J_{ENA}(E)=C/\epsilon\tau EG$$

where G denotes the energy geometric factor for each energy band, ε is the sensor efficiency, and τ is the effective accumulation time. The energy g-factor, the energy band, and the sensor efficiency of the IBEX-Hi sensor are precisely described in Funsten et al. (2009). The sensor accumulation time is the time when the IBEX-Hi FOV was actively pointing to the region of interest.

- ENA and ion fluxes are related by: $J_{ENA}(E,x,z)=\int J_{ion}(E,x,y,z)\sigma(E)n_H(x,y,z)\,dy$ where $J_{ENA}(E,x,z)$ is the observed ENA flux projected in the GSE XZ plane, $J_{ion}(E,x,y,z)$ is the local ion flux, and $\sigma(E)$ is the energy-dependent charge-exchange cross section between energetic proton and ambient hydrogen atoms, calculated from an empirical formula (Lindsay and Stebbings, 2005).

- n_H can be calculated based on empirical models such as a spherical harmonics model obtained by the TWINS1-LAD measurement assuming isotropic Lyman-α resonant scattering (Zoennchen et al., 2011).

3.2 IBEX Magnetospheric Imaging Considerations

- **Spatial/temporal variations** - IBEX instruments have large FOVs, and hence poor spatial resolution (~2 to ~5 R_E along the X_{GSE} and sub-R_E in the Z_{GSE} direction) at any given instant and place where the FOV intersects the XZ meridian plane. Also the spacecraft location and spin axis are not fixed with respect to the Earth and therefore the viewing perspective slowly changes with time. Therefore when creating composite images of the magnetosphere, certain assumptions must be made with respect to the expected ENA emission spatial gradients within the magnetosphere, and the expected time scales of temporal variations across these spatial scales.
- **Line-of-sight integration** - The data for this release is presented under the assumption that most of the ENA emissions occur within the magnetosphere and peak in the noon-midnight meridian plane, which may not always be the case. This complication is true of all imaging of optically thin environments.

- **Pitch angle variations** - Since ENA emissions are assumed to peak near the noon-midnight meridian plane, pitch angles must be close to 90° between the magnetospheric magnetic field and the IBEX instrument field of views, however there may actually be some pitch angle dependencies on ENA emissions that are not considered.

• Data

In addition to the 5 data files associated with each orbit and which correspond to ENA measurements at ~0.71, ~1.11, ~1.74, ~2.73, and ~4.3 keV, we provide a browse plot showing five ENA skymaps, orbital configurations, and a sample interval projected onto the XZ plane (see Figure 3). Each count file contains a descriptive header. Whenever used, the published studies that examined the various orbits should be cited as the referenceable sources for each of these orbits, as indicated in the table in section 2. Data can be downloaded from the table below, which also indicates the start and stop times for each orbit.

Orbits	Orbit Start and End Times
23	2009-03-26 21:09:00.318 to 2009-04-03 16:07:51.743
24	2009-04-03 12:10:21.253 to 2009-04-11 08:15:09.669
25	2009-04-11 05:06:40.967 to 2009-04-18 22:05:11.125
27	2009-04-26 08:27:40.916 to 2009-05-04 05:31:06.519
29	2009-05-19 19:27:18.831 to 2009-05-11 17:27:02.484
51	2009-10-26 08:19:34.905 to 2009-11-03 02:38:01.730
52	2009-11-02 22:34:07.792 to 2009-11-10 19:03:55.230
53	2009-11-10 15:46:22.161 to 2009-11-18 10:58:17.674
55	2009-11-25 23:44:19.069 to 2009-12-03 11:26:37.151
56	2009-12-03 08:22:31.792 to 2009-12-10 22:03:52.604
57	2009-12-10 18:55:33.969 to 2009-12-18 06:58:47.247
72	2010-04-04 11:17:28.386 to 2010-04-12 09:13:51.008
74	2010-04-19 14:09:01.851 to 2010-04-27 03:44:14.913
77	2010-05-12 01:33:51.796 to 2010-05-19 20:43:01.583
78	2010-05-19 17:33:48.047 to 2010-05-27 13:02:03.396
103	2010-11-26 07:56:05.324 to 2010-12-04 04:11:44.879

188b	2012-12-03 12:46:18.859 to 2012-12-08 00:44:50.846
206a	2013-05-13 23:15:27.433 to 2013-05-17 12:19:58.215

Download .zip of all files

• References

Dayeh, M. A., S. A. Fuselier, H. O. Funsten, D. J. McComas, K. Ogasawara, S. M. Petrinec, N. A. Schwadron, and P. Valek, Shape of the terrestrial plasma sheet in the near-Earth magnetospheric tail as imaged by the Interstellar Boundary Explorer, Geophys. Res. Lett., 42, 7, 2115-2122, doi:10.1002/2015GL063682, 2015

Funsten, H.O., F. Allegrini, P. Bochsler, G. Dunn, S. Ellis, D. Everett, M.J. Fagan, S.A. Fuselier, M. Granoff, M. Gruntman, A.A. Guthrie, J. Hanley, R.W. Harper, D. Heirtzler, P. Janzen, K.H. Kihara, B. King, H. Kucharek, M.P. Manzo, M. Maple, K. Mashburn, D.J. McComas, E. Moebius, J. Nolin, D. Piazza, S. Pope, D.B. Reisenfeld, B. Rodriguez, E.C. Roelof, L. Saul, S. Turco, P. Valek, S. Weidner, P. Wurz, and S. Zaffke, The Interstellar Boundary Explorer High Energy (IBEX-Hi) neutral atom imager, Space Sci. Rev., doi 10.1007/s11214-009-9504-y, 146, 75-103, 2009

Fuselier, S. A., H. O. Funsten, D. Heirtzler, P. Janzen, H. Kucharek, D. J. McComas, E. Möbius, T. E. Moore, S. M. Petrinec, D. B. Reisenfeld, N. A. Schwadron, K. J. Trattner, and P. Wurz, Energetic neutral atoms from the Earth's subsolar magnetopause, Geophys. Res. Lett., 37, doi:10.1029/2010GL044140, 2010

Fuselier S. A., M. A. Dayeh, G. Livadiotis, D. J. McComas, K. Ogasawara, P. Valek, H. O. Funsten, and S. M. Petrinec, Imaging the development of the cold dense plasma sheet, Geophys. Res. Lett., doi: 10.1002/2015GL065716, 2015

McComas, D. J., M. A. Dayeh, H. O. Funsten, S. A. Fuselier, J. Goldstein, J. M. Jahn, P. Janzen, D. G. Mitchell, S. M. Petrinec, D. B. Reisenfeld, and N. A. Schwadron, First IBEX observations of the terrestrial plasma sheet and a possible disconnection event, JGR, 116, doi:10.1029/2010JA016138, 2011

McComas D. J., N. Buzulukova, M. G. Connors, M. A. Dayeh, J. Goldstein, H. O. Funsten, S. Fuselier, N. A. Schwadron, and P. Valek, Two Wide-Angle Imaging Neutral-Atom Spectrometers and Interstellar Boundary Explorer energetic neutral atom imaging of the 5 April 2010 substorm, JGR, doi: 10.1029/2011JA017273, 2012

Ogasawara, K., V. Angelopoulos, M. A. Dayeh, S. A. Fuselier, G. Livadiotis, D. J. McComas, J. P. McFadden, Characterizing the dayside magnetosheath using energetic neutral atoms: IBEX and THEMIS observations, JGR, doi: 10.1002/jgra.50353, 2013

Petrinec, S. M., M. A. Dayeh, H. O. Funsten, S. A. Fuselier, D. Heirtzler, P. Janzen, H. Kucharek, D. J. McComas, E. Moebius, T. E. Moore, D. B. Reisenfeld, N. A. Schwadron, K. J. Trattner, and P. Wurz, Neutral atom imaging of the magnetospheric cusps, JGR, 116, doi:10.1029/2010JA016357, 2011

Lindsay, B. G., and R. F. Stebbings (2005), Charge transfer cross sections for energetic neutral atom data analysis, J. Geophys. Res., 110, A12213, doi:10.1029/2005JA011298

Zoennchen, J. H., J. J. Bailey, U. Nass, M. Gruntman, H. J. Fahr, and J. Goldstein (2011), The TWINS exospheric neutral H-density distribution under solar minimum conditions, Ann. Geophys., 29, 2211–2217, doi:10.5194/angeo-29-2211-2011